Imbalance in ALR ubiquitination accelerates the progression of nonalcoholic steatohepatitis to hepatocellular carcinoma

Wei An (anwei@ccmu.edu.cn)
Capital Medical University
Mingzhe Zheng
Ziwei Ai
Yujiao Chen
ping xie
Capital Medical University

Article

Keywords: augmenter of liver regeneration, ubiquitination, non-alcoholic steatohepatitis, hepatocellular carcinoma, mitochondria

Posted Date: July 5th, 2022

DOI: https://doi.org/10.21203/rs.3.rs-1784603/v1

Version of Record: A version of this preprint was published at Oncogene on November 25th, 2022. See the published version at https://doi.org/10.1038/s41388-022-02549-7.

Abstract

Hepatocellular carcinoma (HCC) is the most common form of primary liver cancer. Accumulating evidence indicates that non-alcoholic steatohepatitis (NASH) is a key predisposing factor for HCC occurrence. However, the precise mechanisms driving NASH transition to HCC remain largely obscure. Augmenter of liver regeneration (ALR) is a sulfhydryl oxidase and cytochrome c reductase that functions as an important regulator of mitochondrial dynamics. In this study, we focused on ALR ubiquitination-mediated degradation and its potential contribution to NASH-driven HCC progression at the mitochondrial level. Hepatic ALR expression in HCC patients was determined using immunohistochemical analysis. Mice with liver-specific deletion of ALR (ALR^{CKO}) and ALR^{WT} mice were fed a western diet (WD) and high-sugar solution for induction of NASH. HCC in animals was induced via peritoneal administration of CCl_4. ALR expression was markedly decreased in liver tissues of patients with NASH and HCC compared with non-NASH and non-tumor tissues. Similarly, in ALR^{WT} mice, the ALR level in tumor tissue was reduced relative to that in para-tumor tissue. In the ALR^{CKO} group, mice fed WD plus CCl_4 developed HCC starting at week 12 while ALR^{WT} mice fed WD plus CCl_4 developed HCC at week 24. Analysis of protein posttranslational modifications revealed ubiquitylation (Ub) and deubiquitination (DUb) of ALR by murine double minute 2 (MDM2) and ubiquitin-specific protease 36 (USP36), respectively. Imbalance between Ub and DUb of ALR resulted in profound ALR degradation, which appeared to be reversibly associated with Edmondson-Steiner tumor grade. Rescue of ALR levels via gene transfection abolished tumor malignant features to a certain extent *in vitro*. Notably, *ALR* deletion substantially enhanced mitochondrial fission by activating Drp1 phosphorylation, thus disrupting the balance of mitochondrial dynamics between fission and fusion and severely impairing oxidative phosphorylation (OXPHOS) and ATP synthesis, instead enhancing anaerobic metabolism, which might be attributed to steatotic hepatocyte transition into the malignant HCC phenotype. Hepatic *ALR* depletion via dysregulation of ubiquitination is a critical aggravator of NASH-HCC progression and represents a promising therapeutic target for related liver diseases.

Introduction

Hepatocellular carcinoma (HCC) is the third leading cause of cancer-associated death worldwide [1]. Accumulating studies have disclosed non-alcoholic fatty liver disease (NAFLD) as a significant risk factor for HCC development [2–5]. NAFLD is the most common chronic liver disorder, with reports of an alarming increase in prevalence in association with the obesity epidemic [6]. In the absence of effective treatment, NAFLD can progress to non-alcoholic steatohepatitis (NASH), fibrosis/cirrhosis, and even HCC. Although the molecular mechanisms underlying the onset of NASH-associated HCC remain largely unknown, previous investigations suggest that multiple mechanisms, including stimulation of proinflammatory cytokines, dysregulation of adipokines, oxidative and endoplasmic reticulum (ER) stress as well as altered gut microbiota, contribute to development of NAFLD-mediated hepatocarcinogenesis [7–11]. Therefore, clarification of the molecular pathogenic pathways underlying NAFLD-HCC

development and identification of effective novel targets for therapeutic purposes remain a clinical priority.

Augmenter of liver regeneration (ALR), also known as hepatic stimulatory substance (HSS), was originally identified in weanling or regenerating rat livers [12]. A number of studies have shown that ALR protects the liver from the effects of various toxins, including carbon tetrachloride, D-galactosamine, ethanol, and hydrogen peroxide [13–15]. With regard to association of ALR with HCC, information obtained to date is controversial. Several studies have reported that protein levels of ALR are decreased in liver tissues from patients with NASH [16, 17]. Conversely, other reports suggest that ALR is highly expressed in HCC tissues [18, 19]. An earlier meta-analysis demonstrated an inverse correlation of ALR protein expression with histological angioinvasion and tumor grade of HCC [20, 21]. Moreover, Gandhi et al. reported that mice with hepatocyte-specific *ALR* deletion (ALR^{CKO}) exhibit severe hepatic steatosis shortly after birth progressing to HCC after 12 months, indicating a key role of ALR in the development of HCC from non-alcoholic steatohepatitis [16]. However, the precise mechanisms involved in this process remain to be established. Mitochondria play a crucial role in the switch from NASH to HCC. ALR deficiency impairs not only mitochondrial ultrastructure but also function. For instance, in livers of ALR^{CKO} mice, mitochondrial respiratory capacity is damaged along with ATP synthesis [16]. Ablation of mitochondrial protein mitofusin 2 (Mfn2) in liver induces a NASH-like phenotype and liver cancer, accompanied by reduced transfer of phosphatidylserine from endoplasmic reticulum (ER) to mitochondria [22]. In obesity- and NASH-driven HCC, metabolic reprogramming mediated by downregulation of carnitine palmitoyltransferase 2 enables HCC cells to escape lipotoxicity and promotes hepatocarcinogenesis [23]. The collective results suggest that damage to mitochondrial homeostasis serves as a deteriorating factor that facilitates steatotic hepatocyte transition to HCC.

In this study, hepatic ALR was significantly downregulated in patients with NASH and HCC. The reduction in ALR was negatively associated with pathological grade of HCC. ALR^{CKO} mice fed a western diet with additional CCl_4 challenge developed HCC earlier than their littermates. Mechanistically, decrease in hepatic ALR resulted from enhanced ubiquitination induced by MDM2. Insufficient hepatic ALR expression led to activation of dynamin-related protein-1 (Drp1), thereby exacerbating mitochondrial fission and disrupting mitochondrial dynamics, which accelerated progression of NASH to HCC. Our collective results support a novel regulatory mechanism involving ALR during NASH progression to HCC and highlight its utility as a potential therapeutic target for management of NASH-associated HCC.

Methods And Materials

Human liver samples

Liver specimens from healthy adults (n = 3) and patients diagnosed with NASH (n = 15) were obtained from the Fifth Medical Center of Chinese PLA General Hospital (Beijing), Beijing Friendship Hospital and Beijing You'an Hospital (Beijing, China), respectively. A total of 8 paired HCC and adjacent non-cancerous tissues were obtained from the China-Japan Friendship Hospital. The HCC tissue microarray chip

including 80 pairs of HCC tumor and matched para-carcinoma tissues was purchased from Shanghai Biochip Company Ltd (HLivH160CS02-M-68-70, Shanghai, China). Collection of human samples complied with the guidelines of the Ethics Committee of Capital Medical University and was only performed with informed consent of patients.

Mouse hepatocarcinoma model and *in vivo* experiments

The HCC mouse model was established according to a previously reported protocol [24]. Male ALR^{WT} and ALR^{CKO} mice (8 weeks old) were fed a normal chow diet (ND) with water provided ad libitum or high-fat diet (Dyets, D18061501, Bethlehem, PA, USA) and high sugar solution (23.1 g/L d-fructose; Sigma-Aldrich, G8270, St Louis, MO, USA) and 18.9 g/L d-glucose (Sigma-Aldrich, F0127). Carbon tetrachloride CCl_4 (Sigma-Aldrich, 289116-100 mL) at a dose of 0.2 μL (0.32 μg)/g of body weight or corn oil was injected intraperitoneally once per week, starting simultaneously with diet administration. Mice were divided into following groups: ND/Oil and WD/CCl_4 (6 ALR^{WT} mice for 12, 18 and 24 weeks, 3 ALR^{CKO} mice for 12 and 6 ALR^{CKO} mice for 18 weeks). Animals were anesthetized via intraperitoneal injection with sodium pentobarbital (Nembutal, 90 mg/kg; Ovation Pharmaceuticals Inc., Deerfield, USA) before sacrifice via cervical dislocation at 12, 18 and 24 weeks. Collected liver and serum samples were subjected to further histological staining, serological and molecular analyses.

Ultrasound detection

Liver tumor formation was measured using B-mode ultrasound (Vevo® 2100; Fujifilm VisualSonics, Inc.) with the array transducers (MS550D; Fujifilm VisualSonics, Inc.; mean beam frequency range of 22-55 MHz). Ultrasound was used to detect tumor incidence. The tumor volume was calculated following the formula: tumor volume = (length x $width^2$)/2.

Cell culture and transfection

HepG2 and HEK-293T cell lines were purchased from American Type Culture Collection (ATCC; Manassas, VA, USA). All cells were cultured in Dulbecco's modified Eagle medium (DMEM) with 10% fetal bovine serum (FBS) at 37°C and 5% CO_2. Cell transfection was performed using Lipofectamine 3000 Transfection Reagent (Invitrogen, L3000008, Waltham, WA, USA) or TurboFect Transfection Reagent (ThermoFisher, R0531, Waltham, MA, USA) following the manufacturers' instructions.

Plasmids and small interfering RNA (siRNA)

The plasmid pcDNA3.0-Flag-ALR was constructed and maintained in our laboratory. HA-ub, Flag/Myc-tagged USP36, Myc-tagged MDM2, Myc-tagged HERC5 and Myc-tagged UBAP2L purchased from YouBio (Changsha, China). USP36, MDM2 and control siRNA were acquired from Hanheng Biotechnology (Shanghai, China). The sequences of siRNAs are shown in Supplementary Table 1.

Reverse transcription-quantitative PCR

Total RNA was extracted using TRIzol reagent (ThermoFisher, 15596018, USA) from liver tissues and cells and reverse transcription performed using Vazyme Hiscript QRT super mix (gDNA wiper) (Vazyme, Nanjing, China). qPCR was performed using SYBRGreen Master Mix (Vazyme, Q511-02, China) and analyzed as described previously [25]. The details of the procedures and probes are provided in Supplementary Table 2. Targeted gene transcription levels were calculated by normalization to 18S ribosomal RNA or β-actin expression.

Immunostaining and confocal microscopy

Cells were incubated on a glass-bottomed dish overnight and fixed with 4% formaldehyde for 10 min. After washing in PBS, cells were permeabilized with 0.2% Triton X-100/PBS, blocked in 5% bovine serum albumin (BSA)/PBS, and sequentially incubated with the relevant primary and secondary antibodies. Fluorescent images were captured under a laser confocal microscope (Leica TCS-NT SP8, Germany).

Cycloheximide chase assay and protein half-life analysis

HepG2 cells were plated on six-well culture plates and transient transfection procedures performed as described above. After transfection for 24 h, cyclohexamide (CHX; MedChemExpress; HY-12320, Monmouth Junction, NJ, USA) was added to cells at a final concentration of 50 μg/mL to block new protein synthesis. Cells were collected at the indicated time points for western blot analysis.

Primary hepatocyte isolation, culture and Oil Red O staining

Primary hepatocytes were isolated from 6- to 8-week-old C57BL/6J and *ALR*^{CKO} mice. Briefly, after anesthetization, mice were perfused through the portal vein with buffer solution lacking Ca^{2+} and Mg^{2+}, followed by 0.05% type IV collagenase. After digestion, liver was excised, minced and filtered through a 70 μm filter. Hepatocytes were further separated via centrifugation at 50 × *g* for 1 min twice. Primary hepatocytes were resuspended in DMEM and seeded in 12-well plates. Oleic acid (OA; Sigma-Aldrich, O1008) at a final concentration of 0.5 mM was added to the medium for 12 h to generate a steatotic cell model. Primary hepatocytes were stained with 60% Oil Red O (Sigma-Aldrich, O0625) working solution for 1 min to examine intracellular lipid accumulation.

Immunoprecipitation and immunoblotting

For immunoprecipitation (IP) assays, cells were lysed in HEPES lysis buffer (20 mM HEPES, 50 mM NaCl, 0.5% Triton-X-100 and 1 mM NaF) supplemented with a protease inhibitor cocktail (Roche, 11836170001, Mannheim, Germany). Cell lysates were incubated with the indicated primary antibody (dilution see below) and protein A/G agarose beads (Santa Cruz, sc-2003, CA, USA) overnight at 4°C. Immunoprecipitants were washed three times with lysis buffer before resolving via SDS-PAGE and precipitated proteins detected using immunoblot.

In vivo ubiquitination assays

Cells were lysed in modified lysis buffer (20 mM Tris-HCl, pH 7.5, 150 mM NaCl, 1 mM EDTA, 10% glycerol, 1% Triton X-100) mixed with a protease inhibitor cocktail. The subsequent steps were the same as those for the IP assay.

Mitochondrial preparations

Mitochondria were isolated from HepG2 cells using a Minute™ Mitochondria Isolation Kit for Mammalian Cells and Tissues (Invent Biotechnologies, MP-007, Plymouth, MN, USA).

ATP assay

The ATP levels were detected using CellTiter-Glo® Luminescent Cell Viability Assay (G7570, Promega, Madison, WI, USA) according to the manufacturer's protocol. ATP levels were normalized to protein content and measured by Multimode Microplate Reader (TECAN Spark, Thermo).

Lactate assay

Lysed liver tissues were incubated with Lactate assay kit (Solarbio, BC2235, Beijing, China) for 20min at 37°C, then immediately detected by absorption at 570 nm using Multimode Microplate Reader (TECAN Spark, Thermo).

Glucose assay

Lysed liver tissues were incubated with Glucose assay kit (Solarbio, BC2505, Beijing, China) for 15min at 37°C, then immediately detected by absorption at 505 nm using Multimode Microplate Reader (TECAN Spark, Thermo).

Antibodies

Antibodies against ALR (11293-1-AP, diluted 1:500), USP36 (14783-1-AP, diluted 1:500), MDM2 (27883-1-AP, diluted 1:500), fatty acid synthase (FASN, 10624-2-AP, diluted 1:500), Ki67 (27309-1-AP, diluted 1:2000), F4/80 (28463-1-AP, diluted 1:2000), smooth muscle actin (SMA, 14395-1-AP, diluted 1:1000), Mitofusin 2 (Mfn2, 12186-1-AP, diluted 1:1000), CD34 (14486-1-AP, diluted 1:1000), COX IV (11242-1-AP, diluted 1:1000), glyceraldehyde-3-phosphate dehydrogenase (GAPDH, 60004-1-Ig, diluted 1:1000), goat anti-rabbit IgG-HRP (SA00001-2, diluted 1:5000), and goat anti-mouse IgG HRP (SA00001-1, diluted 1:5000) were purchased from Proteintech (Chicago, IL, USA). Antibodies targeting Drp1 (ab219596, diluted 1:1000) were obtained from Abcam (Cambridge, UK). Antibodies against phospho-Drp1 Ser616 (3455, diluted 1:500) and phospho-Drp1 Ser637 (4867, diluted 1:1000) were acquired from CST (Danvers, MA, USA) and those targeting MDM2 (sc-56154, diluted 1:500) and ubiquitin (sc-8017, diluted 1:500) from Santa Cruz Biotechnology (Santa Cruz, CA, USA). Antibodies against Flag (PM020, diluted 1:1000), Myc (M192-3, diluted 1:1000) and HA (PM020, diluted 1:1000) were purchased from MBL (Nagoya, Japan). Alexa Fluor 488 goat anti-mouse IgG (H+L) (A-11001, diluted 1:200) and Alexa Fluor 594 goat anti-rabbit IgG (H+L) (A-11012, diluted 1:200) were from Invitrogen (Carlsbad, CA, USA).

Statistical analysis

All data are representative of at least three independent experiments. For data showing normal distribution, parametric analysis was performed using the two-tailed Student's t test for two groups. Two-way repeated measures ANOVA was performed for multiple comparisons with two independent variables. One-way ANOVA was used to analyze simple effects followed by Bonferroni post hoc analysis for data meeting homogeneity of variance or Tamhane's T2 analysis for data of heteroscedasticity. Correlations were analyzed using Pearson's analysis. All data are expressed as mean ± SD. Data were considered significant at $p < 0.05$.

Results

ALR expression is decreased during NASH and HCC

To establish the role of ALR in NASH-HCC, we initially examined its expression in livers of patients with NASH and HCC via immunohistochemical (IHC) staining. Hepatic ALR protein levels were considerably lower in livers of patients with NASH relative to healthy adults (Fig. 1A) and similarly decreased in HCC compared with adjacent tissue (Fig. 1B). Analysis of ALR expression in microarray tissues from 80 patients with HCC consistently revealed significantly lower levels in cancer than para-cancerous tissues (Fig. 1C). Additionally, pathological grading of HCC was negatively correlated to ALR expression (Fig. 1D).

Next, HepG2 cells were challenged with OA and cellular ALR levels assayed. ALR was decreased in OA-treated compared to control cells (Supplementary Fig. 1A). To explore the potential role of ALR in hepatocyte steatosis, primary hepatocytes from ALR^{CKO} mice were isolated and treated with OA. The data showed prominent lipid accumulation within hepatocytes lacking *ALR* after OA administration (Supplementary Fig. 1B). A hepatic transcriptome profile assay on livers of ALR^{WT} and ALR^{CKO} mice was further performed. Notably, in livers of ALR^{CKO} mice, Kyoto Encyclopedia of Genes and Genomes (KEGG) pathways related to NAFLD were significantly altered (Supplementary Fig. 1C). Gene Ontology (GO) analysis of lipid metabolism-related pathways in the ALR^{CKO} group indicated significant upregulation of lipid biosynthesis and conversely, downregulation of fatty acid b-oxidation and catabolism (Supplementary Fig. 1D). Moreover, *ALR* knockdown accelerated cell proliferation and migration (Supplementary Fig. 2A–D) while transfection of cells with *ALR* reversed these effects. These results collectively support the involvement of ALR in regulation of NASH progression to HCC.

Hepatocyte-specific *ALR* deletion accelerates NASH development to HCC

To establish the specific function of hepatic ALR in NASH-associated HCC, we generated an animal HCC model in ALR^{WT} and ALR^{CKO}background mice fedND/Oil or WD with additional CCl_4 challenge for a period of 24 weeks (Fig. 2A). After treatment with WD/CCl_4,mice gradually developed steatohepatitis, fibrosis and tumorigenesis [24]. All parameters reflecting hepatic inflammation, fibrosis and liver malignancy (presented in Supplementary Fig. 3A, E, I) were quantitatively evaluated, as shown in

Supplementary Fig. 3 (B–D, F–H, J–L), supporting NASH-HCC progression in model mice (Supplementary Fig. 4A). As shown in Fig. 2B, abdominal ultrasound revealed a solitary mass in *ALR*^{CKO}mice at week 12. None of the mice in the *ALR*^{WT}group developed cancer nodules on the liver surface at week 12 regardless of CCl_4 challenge (Fig. 2C) while six *ALR*^{CKO} mice developed visible tumors at this time-point (Fig. 2D). The data indicate that liver-specific *ALR* knockout accelerates liver tumor onset in NASH mice Moreover, liver surface tumor numbers and nodules were evidently increased under microscopy in *ALR*^{CKO} mice (Fig. 2E–F). Immunohistochemical staining confirmed that tumor tissue was strongly AFP-positive (Fig. 2G–H). In terms of liver damage, steatosis, hepatocyte ballooning, lobular inflammation, and fibrosis in *ALR*^{CKO}mice became progressively worse compared to *ALR*^{WT}mice (Fig. 2C–D, Supplementary Fig. 4A–D). The body weight changes were not significant among mice from all groups (Supplementary Fig. 4E). Liver weight and liver/body weight ratio were markedly higher in *ALR*^{CKO} compared to *ALR*^{WT}mice (Supplementary Fig. 4F–G). Fasting glucose levels were comparable between *ALR*^{WT} and *ALR*^{CKO} mice at the time-points examined (Supplementary Fig. 4H). Total serum cholesterol and low-density lipoprotein levels showed a mild increase in *ALR*^{CKO} mice treated with ND/Oil at week 18and strong increase following WD/CCl_4 administration (Supplementary Fig. 4I–J). Total serum ALT and AST levels were higher in *ALR*^{CKO} relative to *ALR*^{WT} mice (Supplementary Fig. 4K–L). Overall, these results suggest that *ALR* depletion accelerates progression of liver steatosis to malignancy.

ALR interacts with USP36 and MDM2

The above results clearly indicate that lack of ALR expression accelerates HCC occurrence during NASH progression. Therefore, we further focused on the mechanisms causing downregulation of ALR during NASH-HCC progression, starting with analysis of ALR protein stability. In view of the finding that ubiquitination of a protein commonly results in its degradation via the ubiquitin-proteasome pathway, we initially examined the possibility of ALR ubiquitination during hepatic steatosis. As shown in Fig. 3A, treatment with OA induced ALR protein degradation, which was markedly suppressed by MG132, a potent proteasome inhibitor. Next, plasmids containing Flag-*ALR* and HA-Ub were co-transfected into HEK293T cells to further validate ubiquitination of ALR. Co-immunoprecipation (co-IP) experiments clearly disclosed modification of ALR via ubiquitination (Fig. 3B). To identify potential inducers of ALR ubiquitination, Flag-tagged ALR constructs were transiently transfected into HEK293T cells, following which ALR-coupled proteins were immmoprecipitated, separated via gel electrophoresis, and stained. After mass spectrometry analysis (IP-MS) using an anti-Flag antibody and subsequent sorting according to peptide spectrum scores (Fig. 3C–D), several ubiquitin (Ub) E3 ligases and deubiquitinating enzymes (DUb) potentially affecting ALR stability were identified. UbiBrowser (http://ubibrowser.ncpsb.org/) [26,27] was additionally employed to predict Ub E3 ligases interacting with ALR with high confidence (Fig. 3E). Interactive protein candidates, including MDM2, USP36, UBAP2L and HERC5, were selected, and plasmids carrying their coding sequences transfected into HEK293T cells to evaluate ALR expression. Notably, overexpression of MDM2 led to a dose-dependent decrease in endogenous ALR protein expression with no effect on its mRNA level (Fig. 3F–G) while overexpression of USP36 induced a dose-dependent increase in endogenous ALR protein expression, also without affecting

its transcriptional level (Fig. 3H–I). UBAP2L and HERC5 had no significant influence on ALR protein stability (Supplementary Fig. 5A–B). The co-IP assay confirmed interactions of MDM2 and USP36 with ALR (Fig. 3J), which were further supported by immunofluorescence co-localization experiments (Fig. 3K). Our collective findings indicate that MDM2 and USP36 are critical interacting proteins that govern ALR protein stability.

ALR expression is regulated by the E3 ubiquitin ligase MDM2 and deubiquitinase USP36

We subsequently generated a siRNA-mediated MDM2 knockdown construct for transfection into HepG2 cells. As shown in Fig. 4A, interference with MDM2 led to increased ALR protein but had no effect on *ALR* mRNA levels (Fig. 4B). Conversely, USP36 depletion suppressed ALR protein stability without affecting its corresponding mRNA expression (Fig. 4C–D). The CHX (50 μg/mL) assay confirmed a decrease in ALR stability in a time-dependent manner between 0-12 h following CHX exposure (Fig. 4E) while the ALR level was increased upon siMDM2 transfection (Fig. 4F). Consistently, the half-life of ALR was prolonged upon USP36 transfection and suppressed under conditions of USP36 depletion (Fig. 4G–H). The results demonstrate that the E3 ubiquitin ligase MDM2 destabilizes ALR protein, which is efficiently combated by the deubiquitinase USP36.

Our results suggest that both MDM2 and USP36 interact with ALR and contribute to its protein stability. We further investigated whether MDM2 affects ubiquitination of ALR. To this end, HEK293T cells were co-transfected with HA-Ub and Flag-ALR, either alone or in combination with Myc-MDM2. After 36 h of transfection, cells were harvested and Flag-ALR immunoprecipitated. As shown in Fig. 4I, MDM2 overexpression induced a marked increase in ALR ubiquitination and, conversely, its knockdown markedly suppressed ubiquitination (Fig. 4J). Next, we examined the potential effect of USP36 on ubiquitination of ALR. Notably, USP36 overexpression partially abolished ubiquitination of ALR (Fig. 4K) while depletion of USP36 re-augmented ALR ubiquitination (Fig. 4L). On this basis, the *in vivo* ubiquitination assay was conducted to validate the opposite roles of MDM2/USP36 in regulation of endogenous ALR ubiquitination. As shown in Fig. 4M, knockdown of MDM2 clearly decreased endogenous ALR ubiquitination while depletion of USP36 augmented ALR ubiquitination suppressed by MDM2 (Fig. 4N). In view of these findings, we conclude that MDM2 degrades ALR protein via ubiquitination, which can be partially abolished by USP36.

ALR expression is correlated with MDM2 and USP36 in NASH and HCC

To establish whether the ubiquitination of ALR regulated by MDM2 and USP36 is required for progression of NASH to HCC, we examined the expression of MDM2 and USP36 in liver tissues of NASH-HCC ALR^{WT} mice at different time-points. As shown in Fig. 5A, ALR expression was reduced at week 12 and showed a slight increase at weeks 18and 24 (non-tumor tissues). Identical trends in USP36 expression were observed while elevated MDM2 protein expression was sustained between weeks 12 and 24. Data from quantification analysis are presented in Fig. 5B–D. Notably, expression of ALR in liver tumors of mice administered WD plus CCl_4 at week 24 was substantially decreased compared with that in non-tumor

tissue (Fig. 5A–B). Paradoxically, protein levels of MDM2 were higher in tumor than adjacent tissues (Fig. 5A, C). Consistently, immunohistochemical examination revealed a decrease in both ALR and USP36 expression in WD/CCl_4-treated mice relative to their control counterparts during NASH progression, and, conversely, an increase in MDM2 expression compared to the control group fed a normal diet (Fig. 5E–H). The alterations in mRNA levels of *ALR*, *MDM2* and *USP36* were in accordance with changes in the corresponding protein levels at 12, 18 and 24 weeks (Supplementary Fig. 6A–C). Importantly, our findings confirmed significant enhancement of ALR ubiquitination in liver tumors compared with paired para-tumor tissues (Fig. 5I).

Next, we investigated hepatic ALR expression in human samples. As shown in Fig. 6A, ALR levels in tumor tissue were obviously lower in accordance with enhanced MDM2 (Fig. 6B) and decreased USP36 (Fig. 6C) expression. In addition, the ALR level was inversely related to pathological grade of HCC malignancy (Fig. 6D). Moreover, ALR expression was inversely associated with MDM2 but positively correlated with USP36 (Fig. 6E–G). The results collectively indicate that during NASH transition into HCC, ALR serves as a crucial negative regulator of malignancy of steatotic hepatocytes. Moreover, degradation of ALR due to MDM2-induced ubiquitination and inactivation of its counterpart molecule, USP36, favor HCC development.

ALR depletion accelerates progression of NASH to HCC through exacerbation of mitochondrial fission

Transcriptomic analysis further revealed extensive downregulation of OXPHOS pathways and genes in ALR^{CKO} mice (Supplementary Fig. 1C, Fig. 7A). GO terms associated with mitochondrial OXPHOS and ATP synthesis were prominent in enrichment analysis of ALR^{CKO} mice (Supplementary Fig. 7A–C). To establish whether decreased ALR protein stability due to the imbalance between Ub and DUb states induced by MAM2 and USP36 affects mitochondrial dynamics and promotes tumorigenesis, mitochondrial morphology was examined in the NASH-HCC mouse model. Transmission electron microscopy (TEM) revealed that mitochondria in ALR^{WT} mouse liver appeared as elongated tubules and reticular networks (Fig. 7B). The hepatic mitochondrial length in ALR^{CKO} mice was significantly shorter than that in ALR^{WT} mice. Additionally, mitochondria were markedly enlarged although cristae were not visibly lost (Fig. 7B). In terms of the mitochondrial aspect ratio (AR, defined as length/width ratio) mitochondria of ALR^{CKO} mice that had a swollen and rounded shape were decreased, and further reduced following WD/CCl_4 administration (Fig. 7C).

Phosphorylation of Drp1 at Ser616 is a crucial event for its translocation to the outer mitochondrial membrane (OMM) and subsequent execution of mitochondrial fission [28]. Our data showed that Drp1 is responsible for mitochondrial fission and its phosphorylated form (p-$Drp1^{Ser616}$) was remarkably elevated in ALR^{CKO} relative to ALR^{WT} mice (Fig. 7D). Moreover, p-$Drp1^{Ser616}$ was continuously increased with developmental progression of NASH to HCC (Fig. 7D). In contrast, expression of Mfn2, an essential protein for mitochondrial fusion, and phosphorylation status of $Drp1^{Ser637}$ that suppresses mitochondrial fission were simultaneously decreased in ALR^{CKO} relative to ALR^{WT} mice, with evidence of continuously

declining levels during transition of NASH to HCC (Fig. 7D). Western blot data further confirmed immunohistochemistry findings (Fig. 7E). Next, cytoplasm and mitochondrial fractions were prepared to examine the regulatory effects of siRNA-mediated USP36 knockdown on Drp1 phosphorylation and distribution in HepG2 cells. Consistent with previous studies, ALR overexpression led to inhibition of $Drp1^{Ser616}$ phosphorylation but enhanced Drp1 phosphorylation at Ser637. Depletion of USP36 reduced ALR protein levels in both cytoplasm and mitochondria, which is associated with downregulation of p-$Drp1^{Ser637}$ and upregulation of p-$Drp1^{Ser616}$ (Fig. 7F).

Hepatic ATP synthesis was additionally suppressed in ALR^{CKO} mice treated with WD/CCl_4 (Fig. 7G). To determine the effect of ALR deletion on hepatic aerobic glycolysis in mice, glucose consumption and lactate production were examined. As shown in Fig. 7H–I, ALR deletion significantly promoted glucose consumption and lactate production in hepatocytes, which were further increased upon WD/CCl_4 administration. These results indicate that hepatocytes lacking ALR utilize predominant energy-producing strategies, such as glycolysis, for survival which could promote their malignant transformation through the Warburg effect.

Discussion

With the increased global prevalence of metabolic syndrome [29, 30], more individuals are at risk of developing NAFLD, which can lead to progressive liver damage and HCC. However, the liver-specific molecular mechanisms responsible for NAFLD-NASH-HCC progression remain unclear. In the present study, we consistently observed an evident reduction of ALR expression in liver samples of NASH and HCC patients as well as WD/CCl_4-induced NASH-HCC mice. Co-regulation of ALR by the E3 ubiquitin ligase MDM2 and the deubiquitinating enzyme USP36 is essential for its protein stability, which appears critical in governing mitochondrial dynamics. Loss of mitochondrial dynamics favors transition from NASH to HCC in liver. Our results clearly indicate that downregulation ALR is a key step in NASH-HCC progression, supporting targeting of ALR as a promising therapeutic strategy.

Our experiments confirmed a decrease in ALR expression in fatty liver and HCC. ALR levels are reported to be reduced in liver tissues from patients with NASH but increased in those with cirrhosis and HCC [16–19] and negatively correlated with tumor grade and metastasis in HCC [20, 21]. Despite the existing inconsistences, these findings collectively support the significant involvement of ALR in the metabolic function of liver. We believe that the apparent differences in ALR expression are attributable to the experimental conditions used and/or different stages of the disease. Thus, comprehensive investigation of the mechanisms by which ALR expression is regulated at different stages of disease seems an essential prerequisite for understanding its role in hepatic malignancy.

In OA-induced steatotic HepG2 cells, the ALR level was significantly affected by treatment with the proteasome inhibitor MG132, indicating that protein stability of ALR is regulated through the ubiquitin-proteasome pathway. IP-MS and Ubibrowser experiments revealed that ALR is capable of interacting with E3 ligase MDM2 and the deubiquitinating enzyme USP36. MDM2 is an oncoprotein that acts as a key

repressor of p53 [31]. USP36 is a member of the USP family that can cleave ubiquitin-ubiquitin and ubiquitin-protein bonds through its deubiquitinase activity [32]. CHX and *in vivo* Ub/DUb assays revealed that MDM2 ubiquitinates ALR and promotes degradation while USP36 removes ubiquitin and prevents degradation of ALR. Our current findings clearly suggest that the deficiency of ALR as result of ubiquitination could contribute to transition of steatotic liver to the malignant stage. Moreover, IHC staining results of the HCC tissue microarray confirmed significantly lower levels of ALR relative to paired adjacent non-tumor tissues, which conresponds significantly to Pearson's correlation analysis and could therefore be considered a potential pathological index for diagnosis of HCC malignancy.

As reported previously, ALR deficiency resulted in accelerated hepatic lipid deposition, inflammation and fibrosis, which are likely to be associated with deregulation of hepatic mitochondrial structure and function [17]. Mitochondria are highly dynamic organelles undergoing continuous fusion and fission processes that are critical for mitochondrial homeostasis. Mitochondrial fission depends on the cytosolic GTPase Drp1, which is recruited to the outer mitochondrial membrane where it assembles into multimeric ring complexes that form active GTP-dependent mitochondrial fission sites [33]. Mitochondrial fission-related proteins, such as Drp1 and mitochondrial fission factor (MFF), are induced in the liver in high-fat diet (HFD)-exposed obese mice [34, 35], supporting the involvement of impaired mitochondrial dynamics in the pathogenesis of NAFLD [36]. In addition, liver cancer cells lose their dynamic mitochondrial balance, leading to increased fission and decreased fusion and consequently, mitochondrial dysfunction [33]. Experiments from the current study demonstrated that HCC onset in ALR^{CKO} mice fed HFD occurs much earlier relative to ALR control mice. Comparison of ALR levels confirmed that NASH-induced ALR ubiquitination contributes to acceleration of HCC occurrence. However, further experiments employing both ALR knockout and knock-in animal models with NASH are required to capture sufficient data on a signal-cell proteomics basis validating accelerated HCC growth in ALR^{CKO} mice.

Previous studies by our group have demonstrated that ALR inhibits Drp1 phosphorylation and SUMOylation to rescue hepatocytes from ischemia/reperfusion-induced apoptosis, preventing its translocation and preserving mitochondrial function [37, 38]. Here, we showed that during liver steatosis and HCC, ALR also exerts regulatory effects on the mitochondrial dynamic balance through Drp1. Importantly, however, ALR insufficiency-induced disruption of mitochondrial dynamics may be a deteriorating factor impairing OXPHOS of mitochondria, leading to aerobic glycolysis in hepatocytes to facilitate lower energy consumption, which is a crucial characteristic of tumor cells designated the Warburg Effect.

In conclusion, our study provides preliminary evidence that ubiquitination-dependent regulation of ALR by MDM2 and USP36 is inhibited in WD/CCl_4-induced NASH-associated HCC. Downregulation of ALR accelerates the progression of NASH to HCC via disruption of mitochondrial dynamics. Therefore, maintenance of ALR at the physiological level appears essential to prevent malignant transformation of steatotic hepatocytes.

Abbreviations

ALT, Alanine aminotransferase; ALR, Augmenter of liver regeneration; AST, Aspartate aminotransferase; ATP, Adenosine triphosphoate; CCl_4, Carbon tetrachloride; Drp1, Dynamin-related protein-1; DUB, Deubiquitinase; HE, Hematoxylin-eosin; HSS, Hepatic stimulatory substance; IHC, Immunohistochemistry; IP, Immunopurification; IP-MS, Immunopurification and mass spectrometry; LDL, Low density lipoprotein; MDM2, Murine double minute 2; NT, Non-tumour; OXPHOS, oxidative phosphorylation; T, Tumour, ROS, Reactive oxygen species, siRNA, Small interfering RNA; TC, Total Cholesterol; Ub, Ubiquitin; USP36, Ubiquitin specific proteases 36.

Declarations

Author contributions: Study concept and design: XP, AW; acquisition of patient specimens: ZMZ; acquisition of data: ZMZ, AZW, CYJ; analysis and interpretation of data: XP, ZMZ; drafting of the manuscript: ZMZ; XP; study supervision and manuscript revision: AW, PI of project and core revision of manuscript.

Competing interests: None declared.

Grant support: This work was supported by the National Natural Science Foundation of China (NSFC) (No. 32071128).

Ethics approval: Capital Medical University Ethics Committee.

References

1. Jemal A, Bray F, Center MM, Ferlay J, Ward E, Forman D. Global cancer statistics. CA Cancer J Clin. 2011;61:69–90.
2. Younossi ZM, Otgonsuren M, Henry L, Venkatesan C, Mishra A, Erario M, Hunt S. Association of nonalcoholic fatty liver disease (NAFLD) with hepatocellular carcinoma (HCC) in the United States from 2004 to 2009. Hepatology. 2015;62:1723–30.
3. Hashimoto E, Tokushige K. Hepatocellular carcinoma in non-alcoholic steatohepatitis: Growing evidence of an epidemic? Hepatol Res. 2012;42:1–14.
4. Sung H, Siegel RL, Torre LA, Pearson-Stuttard J, Islami F, Fedewa SA, et al. Global patterns in excess body weight and the associated cancer burden. CA Cancer J Clin. 2019;69:88–112.
5. Baffy G, Brunt EM, Caldwell SH. Hepatocellular carcinoma in non-alcoholic fatty liver disease: an emerging menace. J Hepatol. 2012;56:1384–91.
6. Chalasani N, Younossi Z, Lavine JE, Charlton M, Cusi K, Rinella M, et al. The diagnosis and management of nonalcoholic fatty liver disease: Practice guidance from the American Association for the Study of Liver Diseases. Hepatology. 2018;67:328–57.
7. Park EJ, Lee JH, Yu GY, He G, Ali SR, Holzer RG, et al. Dietary and genetic obesity promote liver inflammation and tumorigenesis by enhancing IL-6 and TNF expression. Cell. 2010;140:197–208.

8. Tilg H, Hotamisligil GS. Nonalcoholic fatty liver disease: Cytokine-adipokine interplay and regulation of insulin resistance. Gastroenterology. 2006;131:934–45.
9. Nakagawa H, Umemura A, Taniguchi K, Font-Burgada J, Dhar D, Ogata H, et al. ER stress cooperates with hypernutrition to trigger TNF-dependent spontaneous HCC development. Cancer Cell. 2014;26:331–43.
10. Yoshimoto S, Loo TM, Atarashi K, Kanda H, Sato S, Oyadomari S, et al. Obesity-induced gut microbial metabolite promotes liver cancer through senescence secretome. Nature. 2013;499:97–101.
11. Nakagawa H. Recent advances in mouse models of obesity- and nonalcoholic steatohepatitis-associated hepatocarcinogenesis. World J Hepatol. 2015;7:2110–18.
12. LaBrecque DR, Pesch LA. Preparation and partial characterization of hepatic regenerative stimulator substance (SS) from rat liver. The Journal of physiology. 1975;248:273–84.
13. Mei MH, An W, Zhang BH, Shao Q, Gong DZ. Hepatic stimulator substance protects against acute liver failure induced by carbon tetrachloride poisoning in mice. Hepatology. 1993;17:638–44.
14. Ho DW, Fan ST, To J, Woo YH, Zhang Z, Lau C, et al. Selective plasma filtration for treatment of fulminant hepatic failure induced by D-galactosamine in a pig model. Gut. 2002;50:869–76.
15. Wu Y, Chen L, Yu H, Liu H, An W. Transfection of hepatic stimulator substance gene desensitizes hepatoma cells to H2O2-induced cell apoptosis via preservation of mitochondria. Archives of Biochemistry and Biophysics. 2007;464:48–56.
16. Gandhi CR, Chaillet JR, Nalesnik MA, Kumar S, Dangi A, Demetris AJ, et al. Liver-specific deletion of augmenter of liver regeneration accelerates development of steatohepatitis and hepatocellular carcinoma in mice. Gastroenterology. 2015;148:379–91.
17. Kumar S, Verma AK, Rani R, Sharma A, Wang J, Shah SA, et al. Hepatic Deficiency of Augmenter of Liver Regeneration Predisposes to Nonalcoholic Steatohepatitis and Fibrosis. Hepatology. 2020;72:1586–604.
18. Yu HY, Zhu MH, Xiang DR, Li J, Sheng JF. High expression of 23 kDa protein of augmenter of liver regeneration (ALR) in human hepatocellular carcinoma. Onco Targets Ther. 2014;7:887–93.
19. Thasler WE, Schlott T, Thelen P, Hellerbrand C, Bataille F, Lichtenauer M, et al. Expression of augmenter of liver regeneration (ALR) in human liver cirrhosis and carcinoma. Histopathology. 2005;47:57–66.
20. Dayoub R, Wagner H, Bataille F, Stöltzing O, Spruss T, Buechler C, et al. Liver regeneration associated protein (ALR) exhibits antimetastatic potential in hepatocellular carcinoma. Molecular medicine (Cambridge, Mass.). 2011;17:221 – 28.
21. Jia X, Li Z, Dong L, Sun G, Wang X, Gao J, et al. Lack of hepatic stimulator substance expression promotes hepatocellular carcinoma metastasis partly through ERK-activated epithelial-mesenchymal transition. Laboratory investigation; a journal of technical methods and pathology. 2018;98:871–82.
22. Hernández-Alvarez MI, Sebastián D, Vives S, Ivanova S, Bartoccioni P, Kakimoto P, et al. Deficient Endoplasmic Reticulum-Mitochondrial Phosphatidylserine Transfer Causes Liver Disease. Cell. 2019;177:881–95.

23. Fujiwara N, Nakagawa H, Enooku K, Kudo Y, Hayata Y, Nakatsuka T, et al. CPT2 downregulation adapts HCC to lipid-rich environment and promotes carcinogenesis via acylcarnitine accumulation in obesity. Gut. 2018;67:1493–504.
24. Tsuchida T, Lee YA, Fujiwara N, Ybanez M, Allen B, Martins S, et al. A simple diet- and chemical-induced murine NASH model with rapid progression of steatohepatitis, fibrosis and liver cancer. J Hepatol. 2018;69:385–95.
25. Zhang C, Huang J, An W. Hepatic stimulator substance resists hepatic ischemia/reperfusion injury by regulating Drp1 translocation and activation. Hepatology. 2017;66:1989–2001.
26. Li Y, Xie P, Lu L, Wang J, Diao L, Liu Z, et al. An integrated bioinformatics platform for investigating the human E3 ubiquitin ligase-substrate interaction network. Nat Commun. 2017;8:347.
27. Wang X, Li Y, He M, Kong X, Jiang P, Liu X, et al. UbiBrowser 2.0: a comprehensive resource for proteome-wide known and predicted ubiquitin ligase/deubiquitinase-substrate interactions in eukaryotic species. Nucleic Acids Res. 2022;50:D719-28.
28. Cribbs JT, Strack S. Reversible phosphorylation of Drp1 by cyclic AMP-dependent protein kinase and calcineurin regulates mitochondrial fission and cell death. EMBO Rep. 2007;8:939–44.
29. Estes C, Razavi H, Loomba R, Younossi Z, Sanyal AJ. Modeling the epidemic of nonalcoholic fatty liver disease demonstrates an exponential increase in burden of disease. Hepatology. 2018;67:123–33.
30. Huang DQ, El-Serag HB, Loomba R. Global epidemiology of NAFLD-related HCC: trends, predictions, risk factors and prevention. Nat Rev Gastroenterol Hepatol. 2021;18:223–38.
31. Lane DP, Hall PA. MDM2–arbiter of p53's destruction. Trends Biochem Sci. 1997;22:372–74.
32. Kim MS, Ramakrishna S, Lim KH, Kim JH, Baek KH. Protein stability of mitochondrial superoxide dismutase SOD2 is regulated by USP36. J Cell Biochem. 2011;112:498–508.
33. Begriche K, Massart J, Robin MA, Bonnet F, Fromenty B. Mitochondrial adaptations and dysfunctions in nonalcoholic fatty liver disease. Hepatology. 2013;58:1497–507.
34. Galloway CA, Lee H, Brookes PS, Yoon Y. Decreasing mitochondrial fission alleviates hepatic steatosis in a murine model of nonalcoholic fatty liver disease. Am J Physiol Gastrointest Liver Physiol. 2014;307:G632-41.
35. Du J, Zhang X, Han J, Man K, Zhang Y, Chu ES, et al. Pro-Inflammatory CXCR3 Impairs Mitochondrial Function in Experimental Non-Alcoholic Steatohepatitis. Theranostics. 2017;7:4192–203.
36. Archer SL. Mitochondrial dynamics–mitochondrial fission and fusion in human diseases. N Engl J Med. 2013;369:2236–51.
37. Mansouri A, Gattolliat CH, Asselah T. Mitochondrial Dysfunction and Signaling in Chronic Liver Diseases. Gastroenterology. 2018;155:629–47.
38. Frank S, Gaume B, Bergmann-Leitner ES, Leitner WW, Robert EG, Catez F, et al. The role of dynamin-related protein 1, a mediator of mitochondrial fission, in apoptosis. Dev Cell. 2001;1:515–25.

Figures

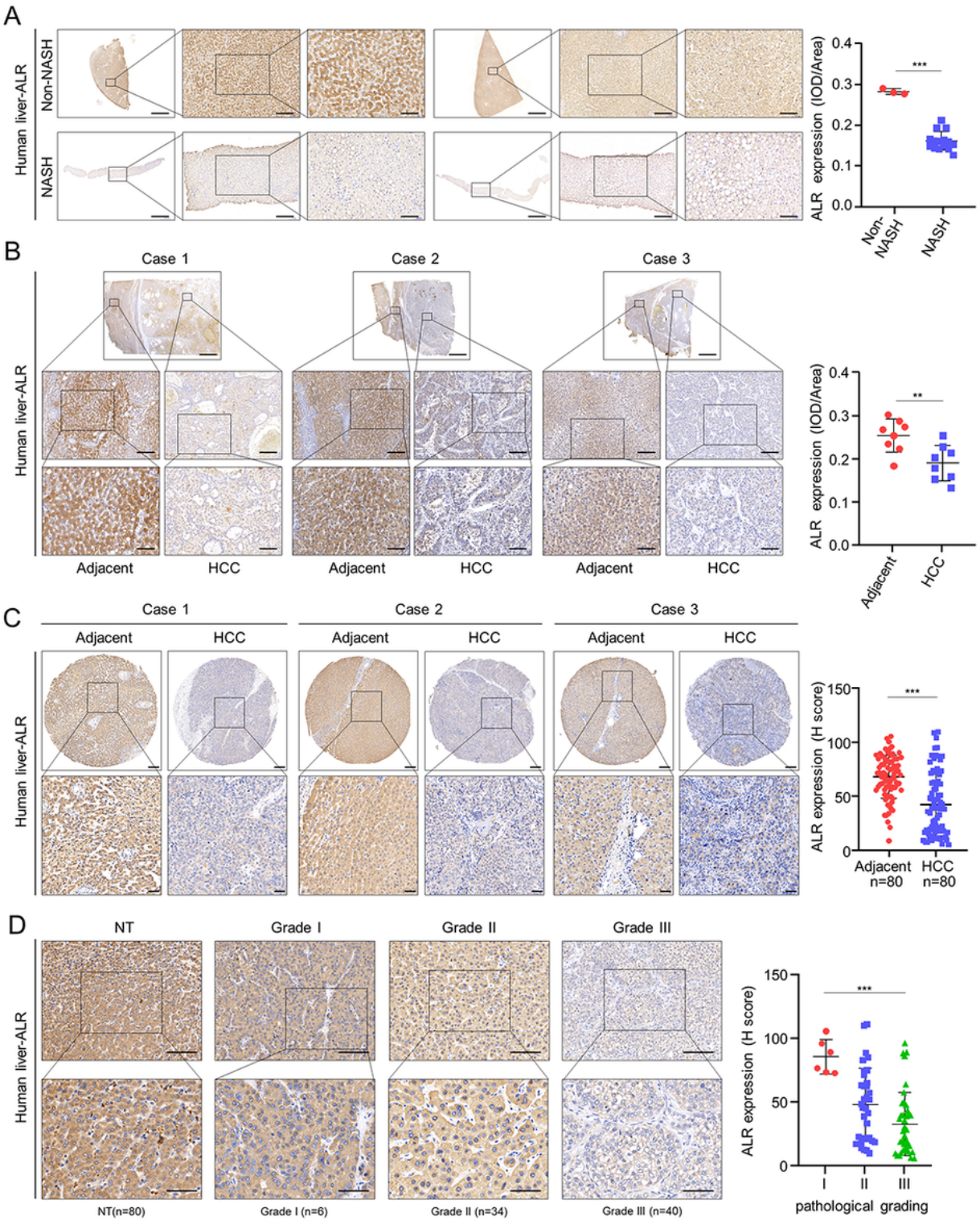

Figure 1

Hepatic ALR expression is decreased in NASH and HCC patients. A Immunohistochemical (IHC) staining images showing a significant decrease in ALR protein expression in livers of NASH patients (n = 15) compared to that in non-steatotic liver samples (n = 3). The intensity of staining was scanned and

scored. Scale bars: 1000, 100 and 50 μm. **B** IHC illustrating ALR protein expression in livers from HCC and paired non-cancerous liver tissues. The intensity of staining was scanned and scored. n = 8 per group. Scale bars: 1000, 100 and 50 μm. **C** Images represent IHC staining and H scores of ALR in 80 paired HCC and matched non-tumor tissues. Scale bars: 200 and 100 μm. **D** Representative images and H scores of ALR staining in accordance with pathological grading of HCC. Scale bars: 100 and 50 μm. P values were calculated with Student's t-test (**A–C**) and two-way ANOVA test (**D**). Data represent mean ± SD.**$p < 0.01$, ***$p < 0.001$. Abbreviations: NASH, non-alcoholic steatohepatitis; HCC, hepatocellular carcinoma.

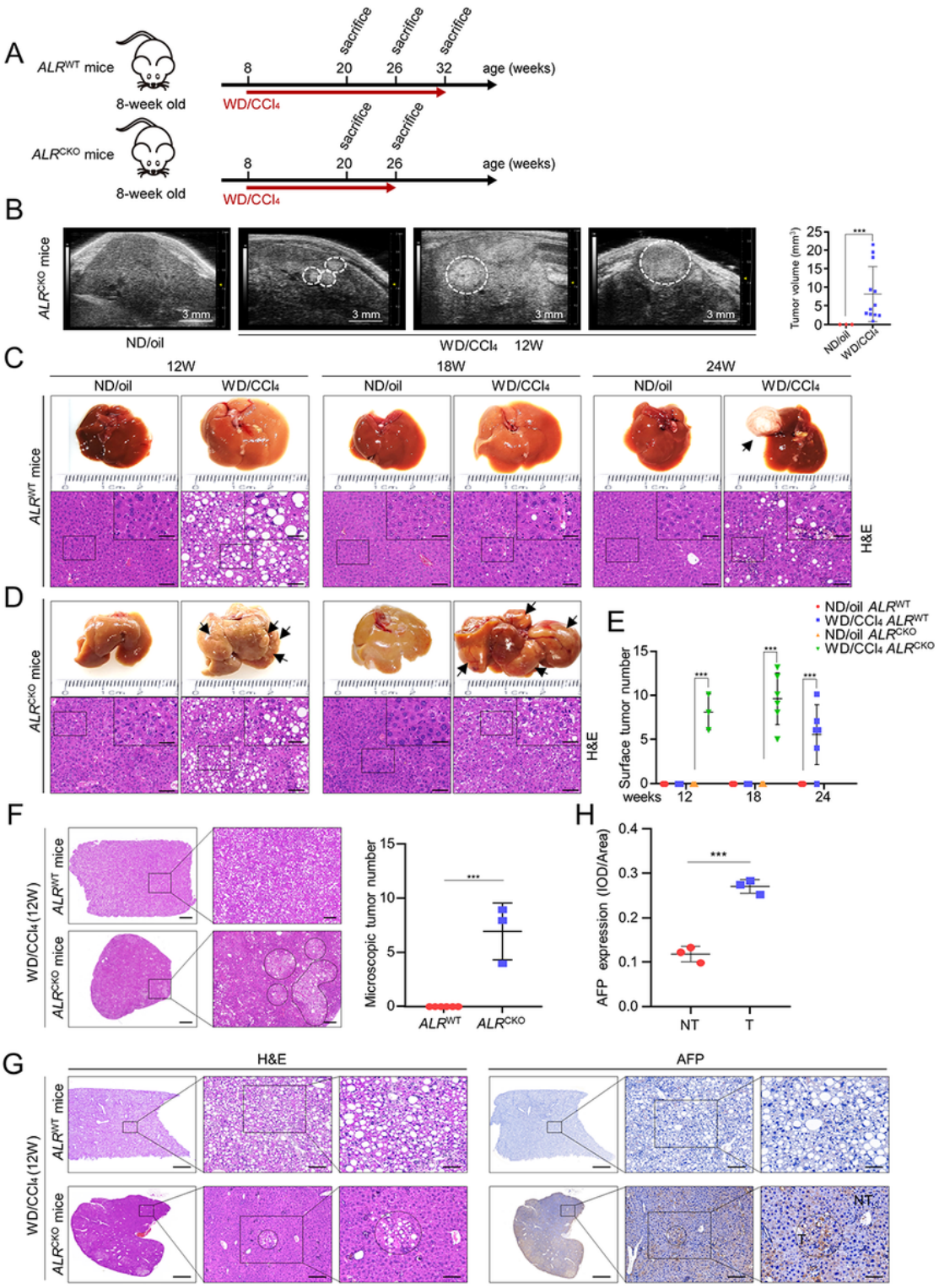

Figure 2

NASH-HCC progression in mice treated with WD plus CCl_4. A Schematic illustration of the NASH-HCC mouse model administered WD/CCl_4. **B** Representative images of liver ultrasound in ALR^{CKO} mice treated with WD/CCl_4 for 12 weeks. Dashed circles represent the ultrasound detection area indicating liver tumor formation. Tumor volumes were calculated using software installed with the ultrasonography machine. Scale bar: 3 μm. **C, D** Representative images of liver surface tumor nodules and Hematoxylin and eosin (H&E) staining from ALR^{WT} and ALR^{CKO} mice fed WD plus CCl_4 for the indicated times. **E** Calculation of surface tumor number per liver in mice treated with WD/CCl_4. **F, G** H&E staining of microtumor nodules in tissue slides. Scale bars: 1000 and 200 μm. Nodule sizes were calculated. **H** AFP expression in liver tissue sections was confirmed via staining and IOD/area ratios of AFP expression determined. Scale bars: 1000, 100 and 50 μm. ND/Oil ALR^{WT}, n = 6; WD/CCl_4 ALR^{WT}, n = 6; ND/Oil ALR^{CKO}, n = 3 (12 weeks); WD/CCl_4 ALR^{CKO}, n = 3 (12 weeks); ND/Oil ALR^{CKO}, n = 6 (18 weeks); WD/CCl_4 ALR^{CKO}, n = 6 (18 weeks). *P* values were calculated with Student's t-test (**B, F, H**) or two-way ANOVA test (**E**). Data represent mean ± SD. ***$p < 0.001$. Abbreviations: CCl_4, carbon tetrachloride; ND, normal diet; WD, western diet; H&E, hematoxylin and eosin; NT, tumor adjacent tissue; T, tumor tissue.

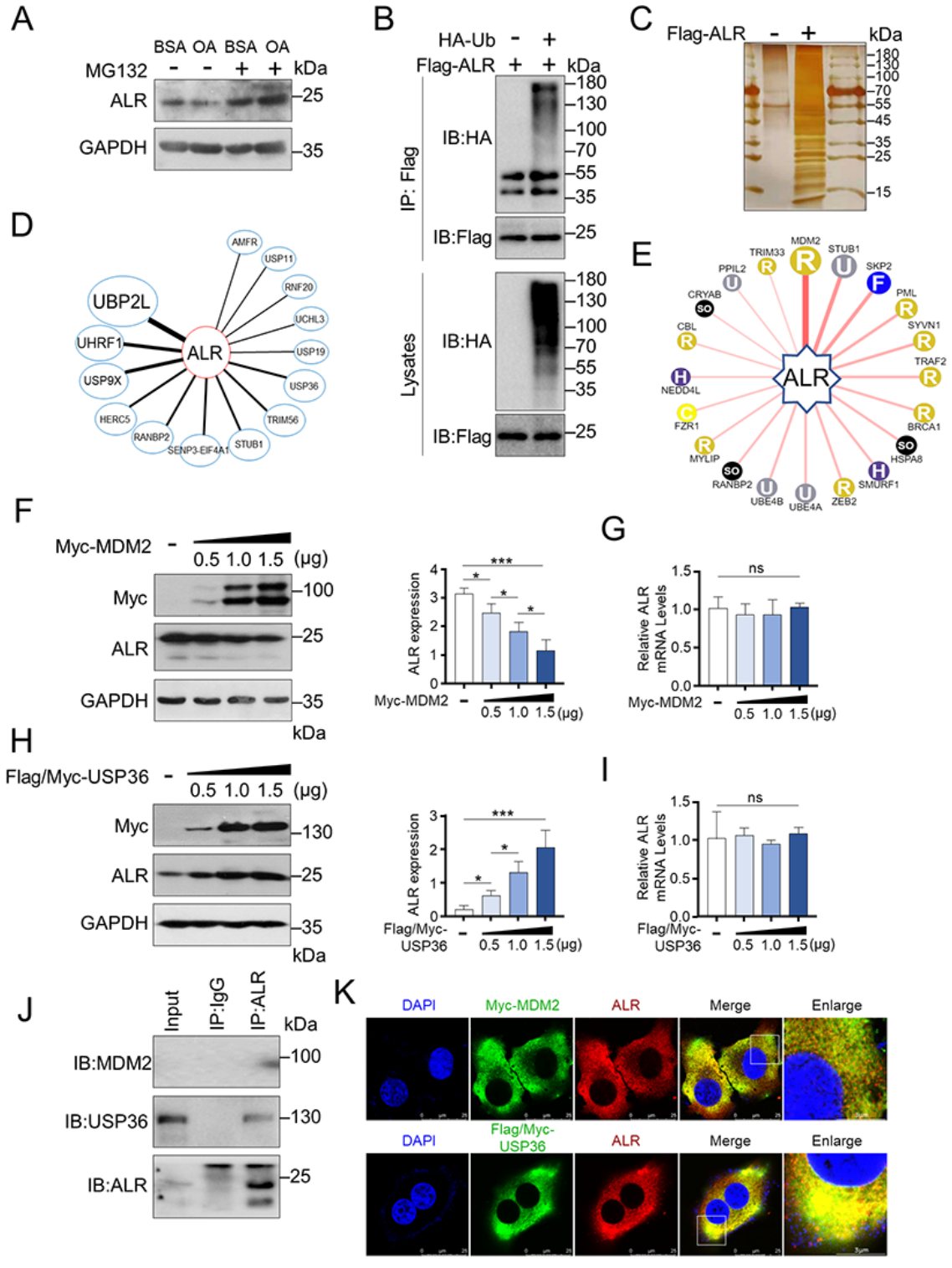

Figure 3

Interactions between ALR and USP36/MDM2. A HepG2 cells were cultured in BSA or oleic acid (OA, 0.5 mM) together with MG132 (10 μM) for 12 h and ALR expression evaluated. **B** Polyubiquitination of ALR in HEK293T cells cultured with MG132 (10 μM). **C** Silver staining of SDS gel loaded with proteins purified using Flag-magnetic beads from Flag-ALR or Flag-vector transfected HEK293T cells. **D** Mass spectrometry analysis of genes encoding ubiquitin E3 ligases and deubiquitination enzymes putatively

interacting with ALR. **E** UbiBrowser was employed to explore the representative predicted E3 ligases that bind ALR. **F** Western blot indicating that ALR expression in HepG2 cells is decreased gradually along with transfection with increasing doses of MDM2 plasmid. GADPH was used for relative quantitation. **G** qRT-PCR analysis of ALR mRNA. **H** Western blot showing that ALR in HepG2 cells is elevated with increasing doses of USP36 plasmid using GAPDH for relative quantitative analyses. **I** qRT-PCR analysis of ALR mRNA. **J** Reciprocal co-IP showing endogenous co-IP of ALR, MDM2 and USP36. **L** HepG2 cells were transfected with Myc-MDM2 or Flag/Myc-USP36C. Immunofluorescence co-localization of Myc (green) and ALR (red) counterstained with DAPI (blue), confirming their mutual interactions. Scale bars: 25 and 8 μm. *P* values were calculated via one-way ANOVA. Data represent mean ± SD.**$p < 0.01$, ***$p < 0.001$. ns, not statistically significant. Abbreviations: Ub, diubiquitin; DAPI, 4',6-diamidino-2-phenylindole.

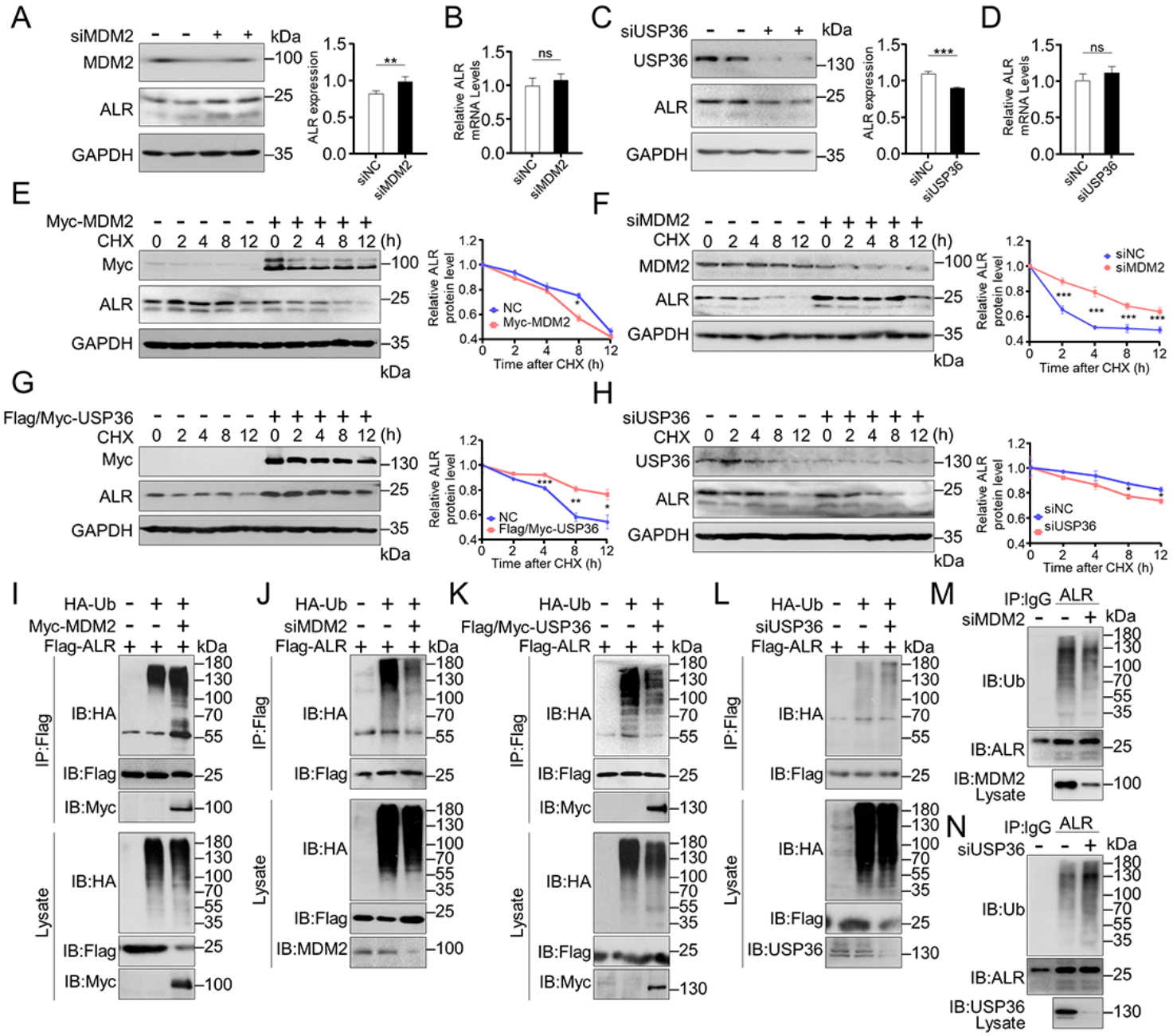

Figure 4

Regulation of ALR by the E3 ubiquitin ligase MDM2 and deubiquitinating enzyme USP36. A, B Following transfection of HepG2 cells with siMDM2, ALR expression modified via MDM2 was analyzed and further quantitated. **C, D** Expression and quantitative analyses of ALR protein in HepG2 cells transfected with siUSP36 plasmid and qRT-PCR of ALR mRNA. **E–H** HepG2 cells transfected with plasmids bearing Myc-MDM2 (**E**), siMDM2 (**F**), Flag/Myc-USP36 (**G**) and siUSP36 (**H**). Cells were cultured with CHX (50 μg/mL) and collected at the indicated times for western blot and quantification of ALR relative to GAPDH. The results clearly indicate that MDM2 ubiquitinates ALR, facilitating protein instability. Transfection of MDM2 siRNA or the DUb UPS36 promoted maintenance of ALR stability. **I–L** Plasmids encoding HA-Ub and Flag-ALR were co-transfected together with the indicated constructs (**I**)/(**K**) or siRNA (**J**)/(**L**) into HEK293T cells and cultured with MG132 (10 μM) for 8 h before harvest. Cell lysates were immunoprecipitated with FLAG Sepharose beads to detect ubiquitin chains on ALR. Following transfection of HepG2 cells with siMDM2 (**M**) or siUSP36 (**N**) and subsequent MG132 treatment, lysates were immunoprecipitated and subjected to immunoblot analysis of ubiquitin. *P* values were calculated with Student's t-test. Data represent mean ± SD. ***$p < 0.001$. Results are expressed as mean ± SD. *$p < 0.05$, **$p < 0.01$, ***$p < 0.001$. ns, not statistically significant. Abbreviations: CHX, cycloheximide.

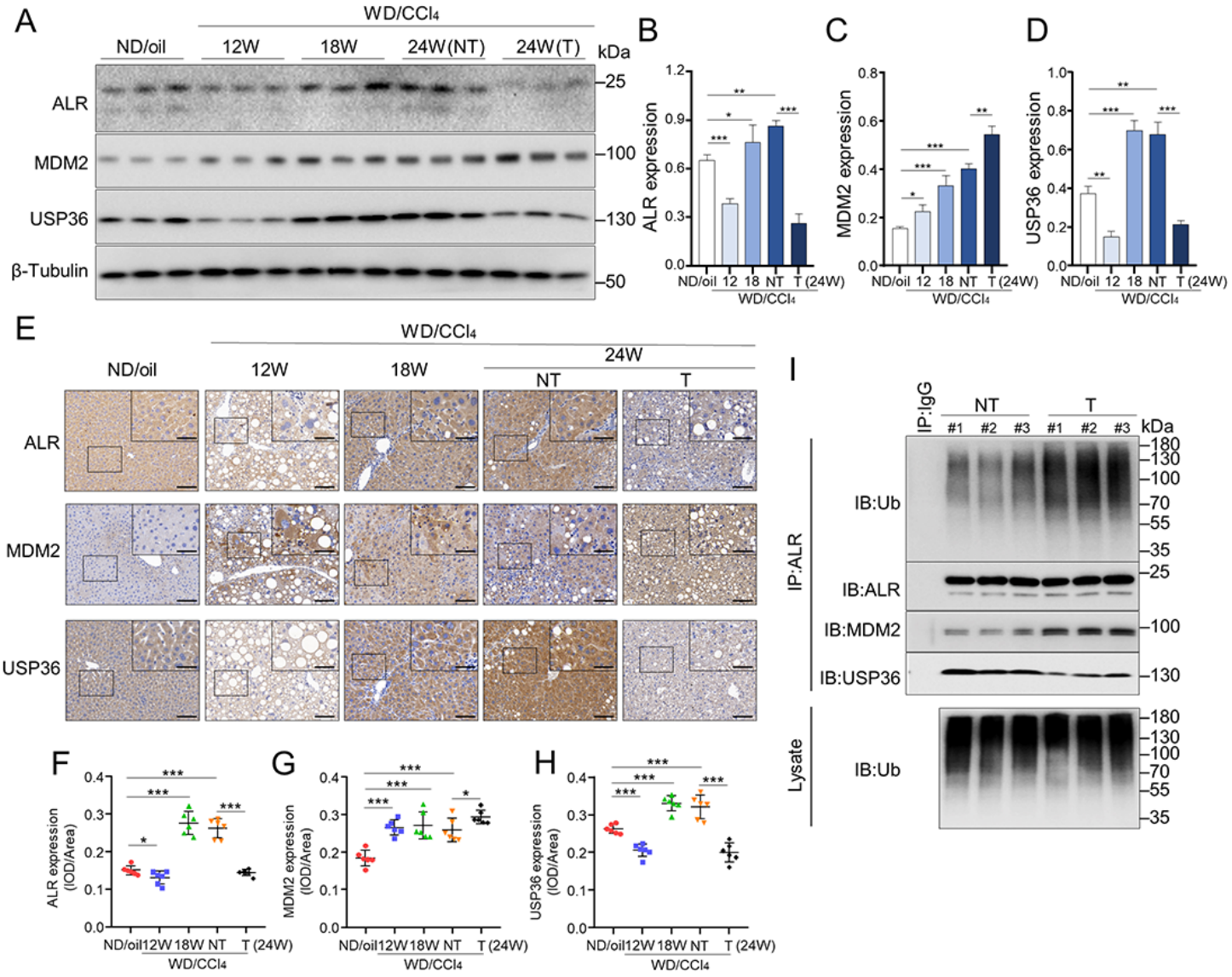

Figure 5

Expression of ALR, USP36 and MDM2 proteins in liver. A Western blot of ALR, MDM2 and USP36 in livers from representative *ALR*^{WT} mice treated with WD/CCl_4 for 12, 18 and 24 weeks using β-tubulin as an internal control (n = 3 per group). **B–D** Quantification of the indicated proteins (n = 3). **E–H** IHC staining results are identical to western blot data (n = 6 per group). Scale bars: 100 and 50 μm. **I** Marked polyubiquitination of hepatic ALR in HCC compared to non-tumor tissue in *ALR*^{WT} mice at 24 weeks. Values are expressed as mean ± SD. *P* values were calculated using one-way ANOVA test. *$p < 0.05$, **$p < 0.01$, ***$p < 0.001$.

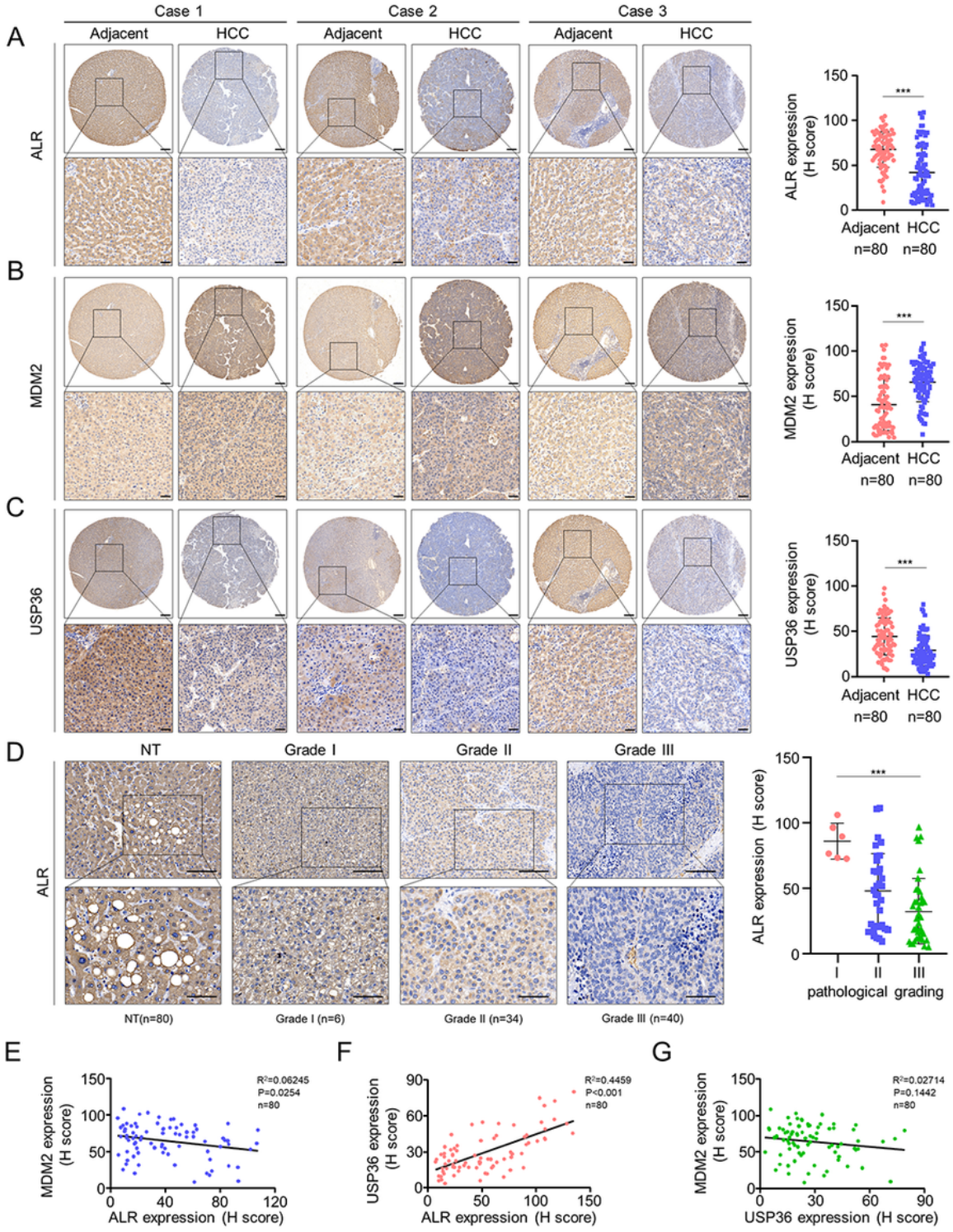

Figure 6

ALR expression is correlated with MDM2 and USP36 in HCC. A–C Representative images and H scores of ALR (**A**), MDM2 (**B**) and USP36 (**C**) in 80 pairs of HCC and matched non-tumor tissues. Scale bars: 200 and 100 μm. **D** Representative images and H scores of ALR at different pathological grades are shown. Scale bars: 100 and 50 μm. **E–G** Correlation analysis of MDM2 (**E**) and USP36 (**F**) with ALR in HCC tissues at the protein level. **G** Correlation analysis between USP36 and MDM2 in HCC tissues. *P* values

were calculated with Student's t-test (**A–C**); one-way ANOVA (**D**); Pearson correlation test (**E–G**). *$p < 0.05$, **$p < 0.01$, ***$p < 0.001$. ns, not significant.

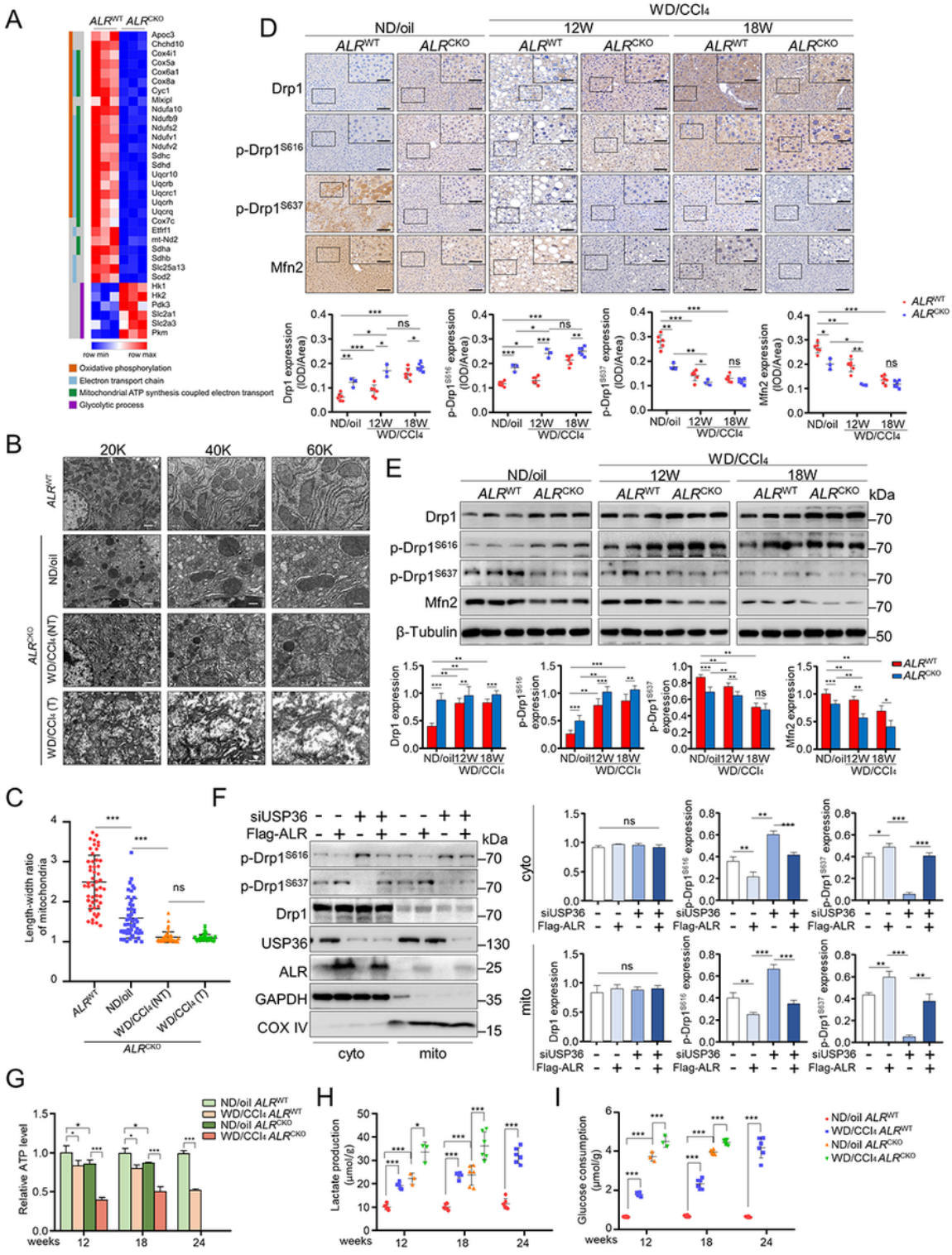

Figure 7

ALR deletion accelerates NASH development to HCC by exacerbating mitochondrial fission and inducing alterations in mitochondrial OXPHOS. A Heatmap of the leading genes involved in OXPHOS pathways of

ALR^{CKO} mice compared to *ALR*^{WT} mice. **B** Transmission electron microscopy images showing severe fragmentation of hepatic mitochondria of *ALR*^{CKO} mice compared to *ALR*^{WT} mice. Scale bars: 1, 0.5 and 0.2 μm. **C** Hepatic mitochondrial length to width ratio is markedly elevated in *ALR*^{CKO} mice according to measurements from 50 cells of each group. **D** IHC staining showing Drp1, p-Drp1^{S616}, p-Drp1^{S637} and Mfn2 protein expression in representative *ALR*^{WT} and *ALR*^{CKO} mice treated with WD/CCl_4 for 12 and 18 weeks. The intensity of staining was scanned and scored. Scale bars: 100 and 50 μm. **E** Western blot depicting Drp1, p-Drp1^{S616}, p-Drp1^{S637} and Mfn2 protein expression in representative *ALR*^{WT} and *ALR*^{CKO} mice treated with WD/CCl_4 for 12 and 18 weeks. **F** Western blot of phosphorylated and total Drp1 in the cytosolic fraction and mitochondrial compartment of HepG2 cells transfected with siUSP36. Cells were transfected with Flag-ALR for the rescue experiment using GAPDH and COX IV as loading controls, respectively. **G** ATP content in mitochondria. **H, I** Lactate production (**H**) and glucose consumption (**I**) were predominantly enhanced in livers of *ALR*^{CKO} mice despite feeding with control diet or WD plus CCl_4. ND/Oil *ALR*^{WT}, n = 6; WD/CCl_4 *ALR*^{WT}, n = 6; ND/Oil *ALR*^{CKO}, n = 3 (12 weeks); WD/CCl_4 *ALR*^{CKO}, n = 3 (12 weeks); ND/Oil *ALR*^{CKO}, n = 6 (24 weeks); WD/CCl_4 *ALR*^{CKO}, n = 6 (24 weeks). Results are expressed as mean ± SD. *P* values were calculated using one-way ANOVA (**C, F**) and two-way ANOVA (**D, E, G–I**). **p* < 0.05, ***p* < 0.01, ****p* < 0.001. ns, not significant.

Supplementary Files

This is a list of supplementary files associated with this preprint. Click to download.

- supplementalmaterial.pdf